

Atmospheric Helium Capillary Dielectric Barrier Discharge for Soft Ionization: Determination of Atom Number Densities in the Lowest Excited and Metastable States

Vlasta Horvatic,[†] Saskia Müller,[‡] Damir Veza,[§] Cedomil Vadla,[†] and Joachim Franzke^{*,‡}

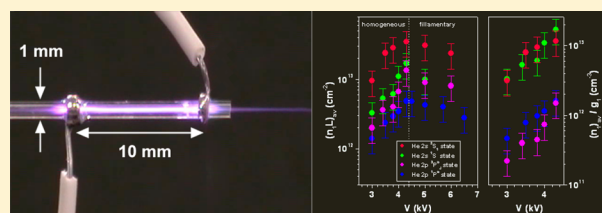
[†]Institute of Physics, Bijenicka 46, 10000 Zagreb, Croatia

[‡]ISAS—Leibniz Institut für analytische Wissenschaften, Bunsen-Kirchhoff-Str. 11, 44139 Dortmund, Germany

[§]Department of Physics, Faculty of Science, University of Zagreb, Bijenicka 32, 10000 Zagreb, Croatia

Supporting Information

ABSTRACT: The populations of the lowest excited helium states $2s\ ^3S_1$, $2s\ ^1S$, $2p\ ^3P^0$, and $2p\ ^1P^0$ created in an atmospheric helium capillary dielectric barrier discharge were determined by means of optical emission spectroscopy. The emitted intensities of 388, 501, 587, and 667 nm lines were measured side-on and end-on with respect to the discharge axis. The comparison of optically thin side-on spectra with end-on spectra, which exhibited the absorption effects in the line kernels, enabled the determination of the average values of the number densities n_1 in the considered He states along the plasma length L . The field of the theoretical profiles for a series of the n_1L parameters pertinent to the experimental conditions was calculated for each line. By introducing the experimental data into the field of calculated curves, n_1L corresponding to the particular state could be obtained. The measurements of the emission profiles were done as a function of the discharge voltage in the range covering homogeneous as well as filamentary DBD operation mode. Due to nonuniformity of the excited atom density distribution along the plasma, the values of n_1 could be obtained only in the homogeneous operation mode where the nonuniformity was small. The following maximum values were found for the number densities in the investigated states: $n_1^{\text{av}}(2s\ ^3S_1) = (2.9 \pm 1.1) \times 10^{13}\ \text{cm}^{-3}$, $n_1^{\text{av}}(2s\ ^1S) = (1.4 \pm 0.5) \times 10^{13}\ \text{cm}^{-3}$, $n_1^{\text{av}}(2p\ ^3P^0) = (1.1 \pm 0.4) \times 10^{13}\ \text{cm}^{-3}$, $n_1^{\text{av}}(2p\ ^1P^0) = (4.2 \pm 1.6) \times 10^{12}\ \text{cm}^{-3}$, and they represent the average populations along the plasma column in the capillary.



In recent years, attention has been focused on the application of plasmas as ambient desorption-ionization (ADI) sources, for the detection of molecular species, capable of producing rapid analytical results with little or no sample preparation.^{1–7} In some of these techniques, dielectric barrier discharges are used for desorption as well as for the ionization process. Experiments have also been carried out on the use of helium-DBDs as ionization sources in ion mobility spectrometry (IMS) and for liquid chromatography/mass spectrometry.^{8–11}

The presence and the involvement of helium metastable atoms are essential not only for better understanding of the mechanisms by which helium-DBDs operate but also for the optimization of their performance for mass spectrometric analyses. It was found that Penning ionization from metastable helium is not the sole ionization pathway for the production of N_2^+ ion in the low temperature plasma (LTP) probe.¹² The authors stressed that they did not want to refute the importance of Penning ionization in the dielectric barrier discharge itself or the plasma jet, which is in their case called afterglow.¹² They meant that a possible important contribution and role of He_2^+ ion in helium-plasma-based ionization sources should also be noted.¹² Since the reported plasma temperatures for all other types of helium discharges used for soft ionization are comparatively low, and do not differ dramatically from the

LTP, they state that it seems to be reasonable to expect that a significant portion of positive charges produced in other helium-plasma-based ambient desorption/ionization sources exists as He_2^+ .¹² Although the study was focused on only one type of discharge used as an ambient desorption/ionization source, the authors meant that it might be possible to apply these findings on fundamental reaction mechanisms to other plasma-based ambient desorption/ionization sources.¹²

We found out that the DBD can be operated in two different modes, the homogeneous and the filamentary mode, which can be recognized by visually monitoring the plasma appearance and simultaneously inspecting the measured plasma current. Filamentary mode shows multiple current peaks, while a homogeneous mode has a well-defined current peak. In the homogeneous mode, the rotational temperature is constant along the discharge axis from the middle of the capillary to the positions in the jet where the N_2^+ 391 band is still measurable. In the filamentary mode, there is a clear increase of rotational temperatures when approaching the anode region, and their values saturate in the jet at about 410 K.¹³

Received: October 21, 2013

Accepted: December 10, 2013

Published: December 10, 2013

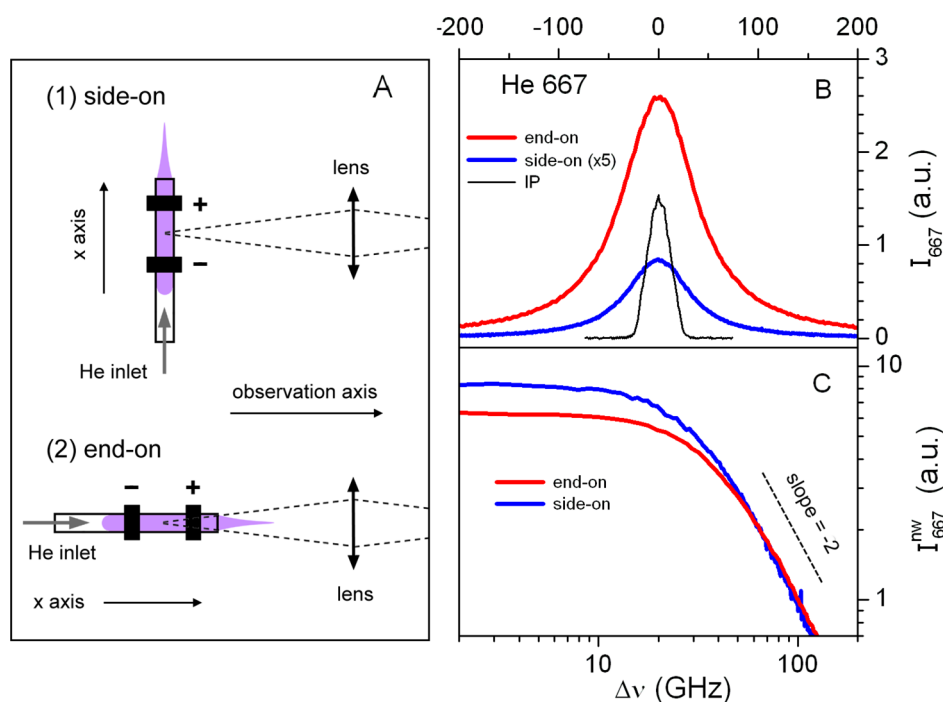


Figure 1. (A) Side-on (1) and end-on (2) geometry. (B) Typical registered signals together with the shape of the instrumental profile (IP). The displayed scans of the He 667 nm line were obtained in the first order of the grating dispersion using 40 μm monochromator slits. The corresponding monochromator band-pass on the wavelength scale amounts to 0.04 nm. The applied voltage amplitudes was $V = 4.3$ kV. (C) The intensities shown in (A) normalized to unity in the optically thin wings at the arbitrary chosen detuning, $\Delta\nu = 100$ GHz, and displayed in double logarithmic scale.

Chan et al. measured comparable or even higher rotational temperatures inside the torch, but outside the torch, the rotational temperature was 550 K.¹² It can be suspected that the plasma is also operated in a filamentary mode and the higher the rotational temperature is, the more He_2^+ are involved.

Therefore, it cannot be argued that if the plasma temperatures for all other types of helium discharges used for soft ionization are comparatively low, and do not differ dramatically from the LTP, that it is reasonable to expect that a significant portion of positive charges produced in other helium-plasma-based ambient desorption/ionization sources exists as He_2^+ .

However, in the common opinion, the soft ionization of analytes starts with N_2^+ molecules, which are directly or indirectly produced by transferring the energy accumulated in helium atoms being in metastable states.^{1,2,7–13} Therefore, the determination of the number densities of helium metastable atoms in a DBD-plasma at atmospheric pressure and their correlation with the efficiency of the produced soft ionization is crucial for understanding the relevant processes. One of the most frequently applied methods for the determination of the densities in the excited atomic states is the laser absorption (see for instance the works of Kunze et al.¹⁴ and Tachibana et al.¹⁵). Unfortunately, the laser systems at our disposal are not able to reach the optical transitions involving the excited helium states of interest. An alternative way to determine the density of metastables in plasma is offered by the application of an atomic emission spectroscopy (AES) method. In principle, the spectral line emission from a plasma volume is followed by simultaneous absorption processes within the plasma. When analyzing a plasma column spectroscopically, the spectral line intensities can be measured perpendicular to a certain position of the column axis (side-on) and along the plasma column

(end-on). By comparison of end-on and side-on spectra, the absorption effects in the line kernels could be detected due to differences in optical paths in the end-on and side-on observed plasma layers. This yields the opportunity to determine the number densities in lower states belonging to the investigated emission lines. However, to apply this OES method for a quantitative absorption analysis, first the appropriate spectroscopic plasma diagnostics including the determination of line profiles, temperature, and electron density in the investigated plasma has to be made. Such an extensive OES investigation of our capillary DBD has been performed,¹⁶ which yielded information that is necessary for the implementation of the method. In the following, the determination of the average number densities in the metastable states $2s\ ^3S_1$ and $2s\ ^1S$ as well in the $2p\ ^3P^o_j$ state and the first resonance $2p\ ^1P^o$ state of helium produced in capillary DBD at atmospheric pressure and various discharge voltages will be presented.

EXPERIMENTAL SECTION

Experiment. The experimental setup used in the present work is the same as in our previous work¹⁷ dealing with operation modes of the capillary DBD operating in helium at atmospheric pressure, and its description will be repeated briefly. Moreover, even the used capillary discharge tube was exactly the same as that used previously.¹⁶

The investigated helium plasma was generated in a capillary quartz tube (outer diameter: 1 mm; inner diameter: 0.5 mm) between two electrodes (electrode distance: 10 mm) surrounding the capillary. The discharge was sustained by a home-built high-voltage generator¹⁸ (pulse duration: 2 μs ; pulse frequency: 21.5 kHz; peak-to-peak voltage: 3–7 kV), and the helium flow was kept at 500 mL/min.

Two experimental geometries with respect to the spectroscopic detection system were applied, which is shown in Figure 1A.

In both cases, the capillary discharge was imaged (imaging ratio: 1:1) by a lens (focal length: 10 cm) to the entrance slit of a 1 m McPherson monochromator having a grating with 1200 grooves/mm, and a thin plasma layer defined by the width of the entrance slit was observed. However, in the first case (side-on), the length of the observed plasma layer was well determined by the size of the inner diameter of the capillary, while in the case of end-on measurements, the effective length of the observed plasma layer was about 20 times larger. The monochromator was supplied either with an RCA-S20 multiplier (red region) or with an EMI S-11 multiplier (UV and blue region). The spectra were obtained by scanning the monochromator, and the obtained signals were stored on a laboratory PC. The emitted spectral line intensities occurring within the period of time of the pulse duration were averaged and recorded as continuous spectra. As an example, the side-on and end-on emission profiles of the He 667 nm line measured at $V = 4.3$ kV is shown in Figure 1B. The side-on intensities were measured near the anode.

The obtained signals show that the end-on spectra exhibit the absorption effects in the line kernel within detuning $\Delta\nu$ of a few tens of GHz. This is demonstrated in Figure 1C where the measured intensities I_{667} , normalized to unity in the wings at arbitrary chosen detuning $\Delta\nu = 100$ GHz, are plotted in double logarithmic scale. Both the side-on and end-on intensities exhibit the same linear dependence (slope: -2) on $(\Delta\nu)^2$ in the line wings. In the case of side-on measurements, the normalized signals I_{667}^{mw} are practically the same in the wings as well as in the line kernel for all investigated discharge voltages. The normalized end-on signals around the line center are reduced in comparison with the signals measured side-on, and this reduction depends on the applied voltage. As will be shown in the next section, this effect can be explained by simultaneous emission and absorption on the optical path along the discharge axis, which is much longer than in the case of the side-on observation

METHOD

Simultaneous Emission and Absorption along the Plasma Column. The influence of simultaneous absorption on the line intensities emitted from a plasma volume is well-known.¹⁹ This effect is in many ways used in plasma diagnostics, and here one of its specific applications is presented. We consider the emission from a plasma column (length: L , diameter: $2r \ll L$), which is observed along its axis x . The plasma is characterized by densities n_1 and n_2 in the states 1 and 2. The intrinsic emission intensity occurring in the transition $2 \rightarrow 1$ in the x -direction from a thin layer of thickness dx at position x can be described by $\varepsilon_{21}(v) dx$, where $\varepsilon_{21}(v)$ is the linear spectral emissivity. The intensity $i_{21}(v, x)$ emitted from the column of length x and incident to the considered thin layer is partially absorbed at the path dx . The amount of the absorbed incident intensity is $k_{21}(v) i_{21}(v, x) dx$, where $k_{21}(v)$ is the linear absorption coefficient.

The difference $di_{21}(v, x)$ between the outgoing and incident spectral line intensity related to the considered thin layer is:

$$di_{21}(v, x) = \varepsilon_{21}(v)dx - k_{21}(v)i_{21}(v, x)dx \quad (1)$$

The frequency-dependent absorption coefficient for the $1 \rightarrow 2$ transition is usually defined by $k_{12}(v) = (\lambda_{12}^2/8\pi) (g_2/g_1) n_1$

$A_{21} P_{12}(v)$. Here, λ_{12} (cm) is the wavelength, g_1 and g_2 are the statistical weights, n_1 (cm^{-3}) is the absorber number density in the state 1, and A_{21} (s^{-1}) is the radiative transition probability for the process $2 \rightarrow 1$. The $P_{12}(v)$ (Hz^{-1}) is the line profile normalized to unity $\int P_{12}(v)dv = 1$. The spectral emissivity $\varepsilon_{21}(v) \propto hv_{12} A_{21} n_2 P_{21}(v)$ in our linear geometry is defined as spectral intensity emitted from the disc-shaped volume $2\pi r^2 dx$ in direction x . The line emission profile $P_{21}(v)$ equals the absorption profile $P_{12}(v)$, which follows from the relationship between the Einstein coefficients for emission and absorption. Expression 1 can be written as

$$\frac{d}{dx}i_{21}(v, x) = k_{12}(v) \left[\frac{\varepsilon_{21}(v)}{k_{12}(v)} - i_{21}(v, x) \right] \quad (2)$$

The ratio $\varepsilon_{21}(v)/k_{12}(v)$ represents so-called source function $S(v)$, and eq 4 is an equation of radiation transfer.¹⁹ If we assume that the plasma is uniform, that is, that the densities n_1 and n_2 as well as the line profile do not depend on the position, then the ratio $\varepsilon_{21}(v)/k_{12}(v)$ can be treated as a constant. In that case, the solution to eq 2 yields the following expression for the resulting spectral intensity related to the length, L , of the whole plasma column:

$$i_{21}(v, L) \propto \frac{8\pi g_1}{\lambda_{12}^2} hv_{21} \frac{n_2}{n_1} \{1 - \exp[-\alpha n_1 L P_{21}(v)]\} \quad (3)$$

where the parameter a ($\text{cm}^2 \text{s}^{-1}$) $= (\lambda_{12}^2 g_2 A_{21}/8\pi g_1)$. If the lines are optically thin ($\alpha n_1 L P_{21}(v) \ll 1$), the corresponding emitted intensity acquires the form $i_{21}(v, L)|_{\text{thin}} \propto hv_{12} A_{21} n_2 L P_{12}(v)$.

Actual profiles in the present experiment are of Voigt type, that is, $P_{12}(v) = P^V(v)$, which is the convolution of Doppler and Lorentz profiles. Voigt function $P^V(\Delta\nu)$ normalized to unit area reads:

$$P^V(\Delta\nu) = \int_{-\infty}^{\infty} P^D(\tau) P_{12}^L(\Delta\nu - \tau) d\tau \quad (4)$$

Here, $\Delta\nu = v - v_{21}$ is the detuning from the line center. The Doppler profile $P^D(\Delta\nu)$ is of the Gaussian form, and normalized to unit area, it can be written as:

$$P^D(\Delta\nu) = \frac{2\sqrt{\ln 2}}{\sqrt{\pi} \Delta_D} \exp \left[- \left(\frac{\Delta\nu}{\Delta_D} 2\sqrt{\ln 2} \right)^2 \right] \quad (5)$$

where $\Delta_D = (2(\ln 2)^{1/2}/\lambda_{12}) (2kT/M)^{1/2}$ is the Doppler fwhm. Here, k , T , and M label the Boltzmann constant, the gas temperature, and the mass of emitting particle, respectively.

The Lorentz component of profile, $P_{12}^L(\Delta\nu)$ normalized to unit area, is given by:

$$P_{12}^L(\Delta\nu) = \frac{1}{2\pi} \frac{\Delta_L}{(\Delta_L/2)^2 + (\Delta\nu)^2} \quad (6)$$

In the above equation, Δ_L (Hz) is the Lorentzian full width at half-maximum (fwhm). The Lorentzian widths are of the form $\Delta_L = \gamma n_p$, where γ (s^{-1}) is the characteristic impact broadening parameter and n_p is the number density of the perturbers producing the line broadening in collisions with emitting particles.

Generally, in the case when $\Delta_L > \Delta_D$, at detuning larger than about $3 \Delta_D$, the Voigt functions acquire the shape of the Lorentzian component. Thus, in the optically thin line wings at

detuning $(\Delta\nu_{\text{wing}})^2 \gg (\Delta_L/2)^2$, according to eq 3, the emitted intensity becomes:

$$i_{21}(\Delta\nu_w, L)|_{\text{thin}} \propto h\nu_{12}A_{21}n_2L \frac{\Delta_L}{2\pi(\Delta\nu_w)^2} \quad (7)$$

When dividing eq 3 by eq 7 at arbitrary chosen $\Delta\nu_N$ in the optically thin Lorentzian wing, the resulting normalized intensity is given by:

$$i_{21}^{\text{nw}}(\Delta\nu, n_1L) = 2\pi \frac{(\Delta\nu_N)^2}{\Delta_L} \frac{1}{an_1L} \{1 - \exp[-an_1LP^V(\Delta\nu)]\} \quad (8)$$

The described procedure of normalization is equivalent to the normalization of the measured spectra in the previous section.

If the line is optically thin in the center also (i.e., if the optical depth $\alpha n_1L P^V(0) \ll 1$), then the normalized intensity i_{21}^{nw} is independent of the product n_1L in the whole spectral range, and it is given by:

$$i_{21}^{\text{nw}}(\Delta\nu) = 2\pi \frac{(\Delta\nu_N)^2}{\Delta_L} P^V(\Delta\nu) \quad (9)$$

According to eq 8, the i_{21}^{nw} gets smaller while increasing the value for n_1L , which is most pronounced in the line center. This explains qualitatively the experimental results given in Figure 1. In the case of end-on measurements ($L = L_{\text{EO}} \approx 10$ mm), the peak of the measured signal is reduced in comparison with the side-on case ($L = L_{\text{SO}} = 0.5$ mm). This is due to absorption in the line kernel which corresponds to the different values for n_1L_{SO} and n_1L_{EO} .

In the case of side-on measurements ($L = L_{\text{SO}} \approx 0.5$ mm), the values of $n_1(V) L_{\text{SO}}$ in the whole range of the applied voltages are sufficiently small, so that the absorption in the line center is negligible. As predicted by eq 9, in that case, the resulting side-on line shapes obtained at various voltages are practically the same (i.e., do not depend on n_1L).

Determination of n_1L Values from Emission Intensities. To enable the comparison of the measured normalized intensities $i_{21}^{\text{nw}}(\nu, n_1L)$ with $i_{\text{CALC}}^{\text{nw}}$ obtained by evaluation of eq 8, it should be taken into account that emitted lines are additionally broadened due to the monochromator instrumental profile $P_{\text{IP}}(\nu)$. After convolving $i_{\text{CALC}}^{\text{nw}}$ with $P_{\text{IP}}(\nu)$, the final expression for the calculated line profile normalized in the line wing, which should be compared with the measured normalized intensities $i_{21}^{\text{nw}}(\Delta\nu)$ reads:

$$I_{\text{CALC}}^{\text{nw}}(\Delta\nu, n_1L) = \int_{-\infty}^{\infty} P_{\text{IP}}(\tau) i_{\text{CALC}}^{\text{nw}}(\Delta\nu - \tau) d\tau \quad (10)$$

By fitting the experimental normalized line profiles $I_{21}^{\text{nw}}(\Delta\nu)$ into the field of $I_{\text{CALC}}^{\text{nw}}(\nu, n_1L)$ lines calculated for a series of n_1L values, the corresponding experimental values for the product n_1L can be obtained.

Equation 8 is derived under the assumption that the number densities n_1 and n_2 as well as the profiles $P_{21}(\nu)$ are independent of the position x along the plasma column. In the present experiment, we were not able to determine the position-dependent behavior of the number densities n_1 in the lower excited states. As for the n_2 densities, this information can be obtained from side-on measurements of the peak emission intensities as a function of x , which is shown in Figure 2, where

the He 667 nm line is again taken as an example. The intensity distributions of other investigated lines are of the similar form.

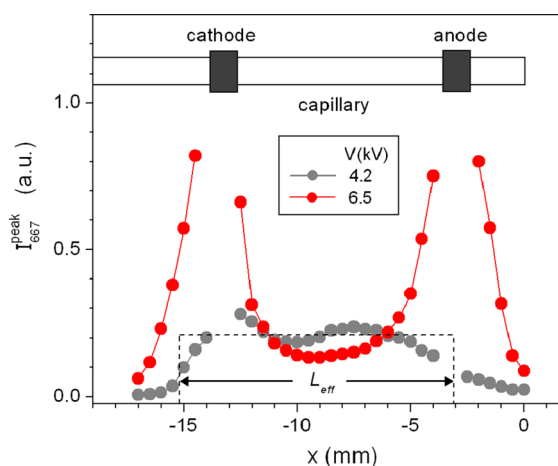


Figure 2. Peak intensities of the He 667 line measured side-on at two different voltages along the x -axis. At 4.2 kV and 6.5 kV, DBD operates in the homogeneous and filamentary mode, respectively. The dashed rectangle is the approximation of the real intensity distribution in the homogeneous mode, having the same area under the curve as the measured one but constant intensity and effective length L_{eff} .

The measured intensity distributions are strongly position-dependent, which reflects the nonuniformity of the discharge column regarding the electron density and electron-impact excitation processes. However, this nonuniformity is less pronounced at lower voltages, which is shown in Figure 2 where the intensity distributions obtained at 4.2 and 6.5 kV are depicted. Distribution shapes very similar to that at 4.2 kV were obtained at lower voltages down to the ignition threshold at about 3 kV. As previously reported,¹⁷ this low-voltage region is attributed to the homogeneous operation mode of the DBD. By increasing the voltage above 4.3 kV, the DBD starts to operate in the filamentary mode with quite different properties than below this threshold. Among other differences, the line intensity distributions along the capillary become strongly dependent on the x position, with the highest intensities appearing in the electrode regions, as shown in Figure 2 for the case of $V = 6.5$ kV.

It is a reasonable assumption that the n_1 -distributions in the lower excited states along the discharge axis are similar to the n_2 -distributions of higher excited states. In this sense, the plasma is nonuniform, and when applying the presented method for our experimental conditions, the measured absorption effects can be attributed only to average values $(n_1L)_{\text{av}}$. In the case of measurements performed with DBD operating at lower voltages (i.e., in the homogeneous mode) the intensity distribution $I_{667}^{\text{peak}}(x)$ along the discharge axis can be approximately replaced by a rectangle having the same area as the area under the real distribution. With the height of this rectangle chosen to be equal to the mean value of intensities between the electrodes, the corresponding length, L_{eff} amounts to about 12 mm. The average number densities along the path L_{eff} can be estimated as $(n_1)_{\text{av}} = (n_1L)_{\text{av}}/L_{\text{eff}}$. In the case of a filamentary discharge, the excited atoms are grouped mainly in two regions around the electrodes, which do not allow such simple approximation as proposed for the measurements in the homogeneous mode.

On the other hand, according to the findings in our previous work,¹⁶ the profiles of the investigated helium lines do not depend on the position. The lines emitted from the capillary DBD are basically characterized by Lorentzian shapes. It was found that the Stark contribution to the Lorentzian broadening is negligible so that the nonuniformity of the electron concentration does not affect the line broadening. The Lorentzian broadening is essentially characterized by the interaction between excited helium atoms and the helium ground state atoms. In the whole range of the applied voltages from 3 kV to 7 kV, the Lorentzian fwhms Δ_L were found to be independent of the position along the discharge axis. The corresponding Lorentzian widths are of the form $\Delta_L \approx \gamma_{\text{HE}} n_{\text{HE}}$, where the number density n_{HE} of the helium ground state atoms is constant along the capillary and defined by atmospheric pressure and room temperature.

MEASUREMENTS AND RESULTS

Measured Helium Lines. The partial term diagram of helium with the transitions involving the lowest excited helium states is given in Figure 3. In the course of the present experiment, the absorption effects related to helium emission lines at 388, 501, 587, 667, 706, and 728 nm were investigated.

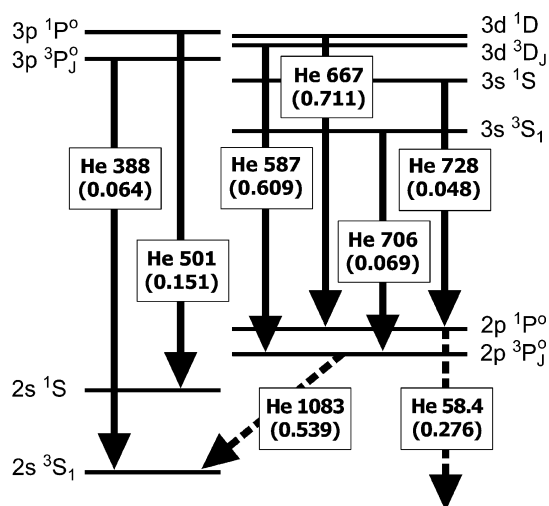


Figure 3. Lowest lying helium excited states and relevant transitions. Black arrows indicate the transitions belonging to the lines measured here. In addition, the lines which are not in the spectral range of our detection system (the resonance line at 58.4 nm and the transition at 1083 nm) are represented by dashed arrows. Numbers in brackets are the line oscillator strengths taken from ref 20.

Absorption effects were detected for helium lines at 388, 501, 587, and 667 nm. In the case of the lines at 706 and 728 nm, the absorption effects were at the edge of the detection limit. These lines have common lower levels with the 587 and 667 nm lines, respectively, and their negligible absorption is a consequence of much smaller oscillator strengths in comparison with the 587 and 667 nm lines.

Other relevant line parameters for four helium lines measured here are taken from Wiese et al.²⁰ and are listed in Table 1. Two of these lines are singlets (at 501 and 667 nm), while the other two exhibit the fine structure. The tabulated parameters for 388 and 587 nm multiplets are related to the overall multiplet values. Table 1 comprises also the data for the Lorentzian widths Δ_L^{atm} measured at atmospheric pressure and

Table 1. Data for the Investigated Spectral Lines^a

λ (nm)	E_1 (cm^{-1})	g_1	g_2	A_{21} (10^3 s^{-1})	Δ_L^{atm} (GHz)	Δ_D^{rt} (GHz)	Δ_{IP} (GHz)
388.8	159 856	3	9	0.095	39 ± 7	4.8	22
501.5	166 278	1	3	0.13	44 ± 4	3.7	25
587.6	169 087	9	15	0.71	35 ± 4	3.2	18
667.8	171 135	3	5	0.638	68 ± 4	2.8	28

^a E_1 : energy of the lower level of the transition; g_1 , g_2 : statistical weights; A_{21} : radiative transition probabilities,²⁰ and relevant fwhms. Δ_L^{atm} : Lorentzian fwhm due to helium self-broadening at atmospheric pressure,¹⁶ Δ_D^{rt} : Gaussian fwhm at $T = 300$ K, Δ_{IP} : fwhm of the actual instrumental profile.

room temperature,¹⁶ the Doppler widths Δ_D^{rt} at $T = 300$ K, and the widths Δ_{IP} of the instrumental profile in the particular case. All lines were measured using 40 μm wide monochromator slits. The helium 667 nm line was measured in the first order of the grating dispersion, 587 and 501 nm lines were measured in the second order, while 388 nm line was measured in the third order.

In the following, the theoretical modeling of the observed line profiles as a function of $n_1 L$ and the evaluation of its average value $(n_1 L)_{\text{av}}$ along the plasma column are presented. It has to be noted that the intensities measured end-on, besides the emission from the capillary, comprise the contribution due to emission from the jet. However, the intensities in the jet are more than 1 order of magnitude weaker than in the capillary.¹⁷ Therefore, this contribution can be safely neglected and the measured end-on intensities can be entirely ascribed to the emission from the capillary.

The fine structures of multiplet 388 and 587 nm lines, the corresponding spectroscopic parameters, and the data relevant for the fitting procedure are given in Supporting Information.

He Absorption in the Metastable $2s \ ^3S_1$ and $2s \ ^1S$, Resonance $2p \ ^1P^o$, and $2p \ ^3P^o$ States. The calculation of theoretical profiles of the measured helium lines was performed according to eq 10, using the program Mathcad 2001 Professional. In the modeling, the Doppler profile P^D with $T = 300$ K¹⁶ was used. The measured instrumental profiles P_{IP} could be very well reproduced with a Gaussian having the fwhm equal to Δ_{IP} , and in the numerical evaluation this analytical form of instrumental profile was used. For each He line, the calculations were carried out with fixed corresponding values for Δ_D and Δ_{IP} listed in Table 1, while the Lorentz width Δ_L was left as a free parameter. The value of Δ_L was varied till the best agreement with the particular experimental profile measured side-on (optically thin) was obtained.

The results of the determination of $(n_1 L)_{\text{av}}$ for 388 nm line are displayed in Figure 4. The best fit to the experimental side-on data in the line kernel was obtained for $\Delta_L = 35$ GHz. With this best Δ_L value, the profiles were calculated according to eq 10 for a series of $n_1 L$ parameters in the range from 10^{10} cm^{-2} to 10^{13} cm^{-2} . Figure 4A displays these theoretical profile curves, together with the normalized profiles measured side-on and end-on at $V = 4.3$ kV. In Figure 4B, the results are shown in double logarithmic scale where the agreement between the measured and calculated profiles can be better discerned.

By using the field of calculated $[I_{\text{CALC}}]_{388}$ curves, the value $(n_1 L)_{\text{av}} = (3.5 \pm 0.7) \times 10^{13} \text{ cm}^{-2}$ was obtained for He 388 nm line in the case of $V = 4.3$ kV. The accuracy of this value is about 20% and is caused by the imprecision introduced with normalization by a relatively weak intensity in the line wing. With $L_{\text{eff}} = (1.2 \pm 0.2) \text{ cm}$, this result yields $(n_1)_{\text{av}} = (2.9 \pm 1.1)$

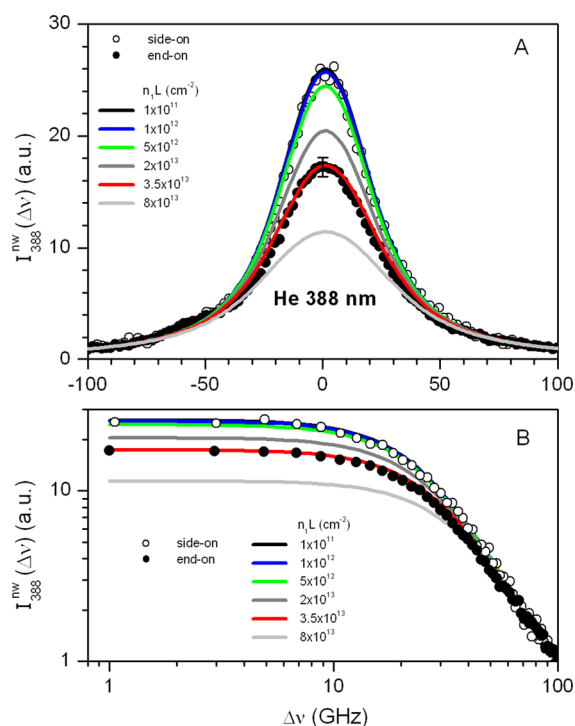


Figure 4. Evaluation of the average value of n_1L in the case of the He 388 nm line. (A) Experimental side-on and end-on (obtained at $V = 4.3$ kV) profiles (dots) together with the profiles calculated for a series of n_1L values (lines). Common experimental error bar is indicated on the end-on measured intensity. (B) The data from (A) plotted in double logarithmic scale.

$\times 10^{13} \text{ cm}^{-3}$ for the number density created in the helium metastable $2s \ ^3S_1$ state at the operating voltage at hand. The atom density accumulated in the $2s \ ^3S_1$ state is the highest of all low lying excited He states considered here.

The measurements performed on 501, 667, and 587 nm lines were analyzed in the same way as presented for the 388 nm line, yielding the results for the average populations along the plasma column in the capillary created in the metastable $2s \ ^1S$, resonance $2p \ ^1P^o$ and $2p \ ^3P^o_j$ states, respectively. The details of these evaluations are given in Supporting Information. The following maximum values were found for the number densities in the investigated states: $n_1^{\text{av}}(2s \ ^1S) = (1.4 \pm 0.5) \times 10^{13} \text{ cm}^{-3}$, $n_1^{\text{av}}(2p \ ^3P^o_j) = (1.1 \pm 0.4) \times 10^{13} \text{ cm}^{-3}$, $n_1^{\text{av}}(2p \ ^1P^o) = (4.2 \pm 1.6) \times 10^{12} \text{ cm}^{-3}$.

The influence of the He flow rate on the obtained results for the atom number densities in the lowest excited and metastable states of helium was checked by varying the flow in the range of 250–1000 mL/min, and no significant effects were observed.

The values of the Lorentz widths Δ_L^{atm} of the investigated lines listed in Table 1 were obtained¹⁶ from the analysis of the line wings of the profiles normalized to unit area. The present Δ_L values which yielded the best match to the experimental results ($\Delta_L = 35, 44.5, 33,$ and 65.5 GHz for 388, 501, 587, and 667 nm lines, respectively) are in very good agreement with Δ_L^{atm} for all the lines considered.

The data for voltage-dependent $(n_1L)_{\text{av}}$ values obtained in the present experiment for all four investigated He lines are shown in Figure 5A. The dashed line at 4.4 kV indicates the transition region between the homogeneous and filamentary operation mode of the DBD.

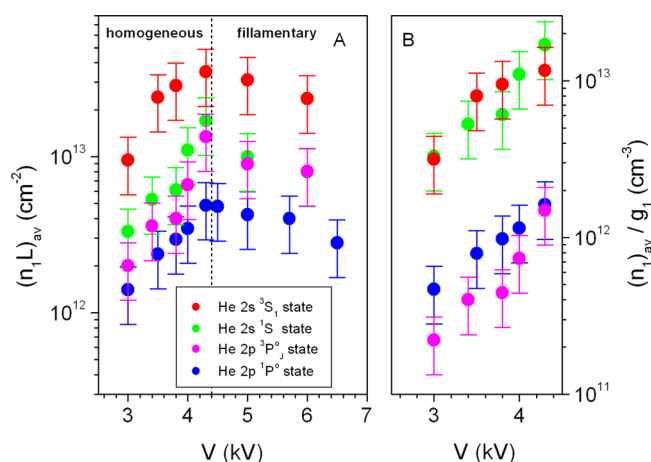


Figure 5. (A) Determined values of $(n_1L)_{\text{av}}$ related to the four lowest excited states of helium as a function of the voltage of the capillary DBD. Vertical dashed line indicates the border between DBD working modes—homogeneous and filamentary. (B) Statistically weighted average number densities $(n_1)_{\text{av}}$ of the considered states measured as a function of the discharge voltage in the homogeneous operation mode.

As discussed in the previous section, the densities of the excited helium atoms in the homogeneous mode can be regarded as nearly constant along the capillary, and the average number densities can be determined using the measured values for $(n_1L)_{\text{av}}$ and the estimated value L_{eff} for the effective length of the plasma. The $L_{\text{eff}} \approx 1.2$ cm is nearly the same at all voltages in the homogeneous mode. In contrast to the homogeneous mode, all measured values for $(n_1L)_{\text{av}}$ decrease with increasing voltage in the filamentary mode, which is most probably caused by shortening of the effective plasma length. In the filamentary mode, the excited He atoms are mainly located around the electrodes. It should be stressed that these distributions around the electrodes become narrower with increasing voltage. Because of the sharp changes of the excited helium atom population along the capillary, the estimation of the effective plasma length, and thus the relevant number densities in the filamentary mode, remains within the framework of speculation.

DISCUSSION

The present measurements show that besides the absorption related to two metastable He S states, the comparable absorption effects occur due to populations in the first two excited P states as well. This populations result from the particular excitation and de-excitation processes, where the effective lifetimes of the considered states under present experimental conditions play an important role. The radiative lifetimes of helium metastables are extremely long, and for unperturbed atoms, amount to several hours. In the experimental conditions at hand, the metastable atoms are destroyed by collisions with ground state atoms, electrons, and the capillary wall. For instance, according to data published by Phelps,²¹ the lifetimes of helium metastables at room temperature and helium atmospheric pressure are reduced to the order of magnitude of microseconds by collisions with ground state atoms. On the other hand, the natural radiative lifetimes of helium 1P and 3P states considered here are short and amount to 0.5×10^{-9} and 1×10^{-7} s, respectively.²⁰ However, their actual lifetimes are much longer than these values, which is due to radiation trapping.^{22–25} Radiative

trapping is a volume effect which is caused by multiple emission, absorption, and re-emission of photons before they leave the zone of excited atoms. Therefore, the effective lifetimes are essentially determined by the size of emitting volume, the number densities in relevant lower states, and the line shapes. This effect is expected to be most pronounced in the case of the resonance ^1P state which is radiatively coupled with the ground state with large population density ($2.6 \times 10^{19} \text{ cm}^{-3}$). For example, in the case of the argon resonance state investigated in a DBD at relatively low pressure,¹⁴ the radiation trapping led to an increase of the effective lifetime to about 4 μs . As for the He ^3P state, it can be expected that the radiative trapping is less effective than in the case of the resonance He ^1P state. The ^3P state is radiatively coupled with the metastable He ^3S state population, which is 6 orders of magnitude smaller than the ground-state atom density. Nevertheless, it seems that the present metastable number density of the He ^3S is sufficiently large to produce the radiation trapping of the He 1083 nm line and corresponding increase of the lifetime of the ^3P state.

To get better insight into the relationship between populations of S and P states, it is useful to take into account the corresponding statistical weights. In Figure 5B, the values $(n_1)_{\text{av}}/g_1$ obtained in the homogeneous operation mode are plotted against the applied voltage. In contrast to data presented in Figure 5A, the number densities weighted by statistical weights are clearly separated into two data sets related to the S and P states. In the equilibrium of the excitation and de-excitation processes, the values for $(n_1)_{\text{av}}/g_1$ should follow the Boltzmann distribution $(n_1/g_1) \propto \exp(-E_1/kT_{\text{exc}})$, but it is obvious that the present results strongly deviate from that expectation. The weighted number densities in the metastable states are nearly the same within the mutual error bars. As generally expected regarding the excitation energy E_1 , the $(n_1)_{\text{av}}/g_1$ of P states are significantly lower than those of the metastable states. However, the ^3P state is underpopulated in comparison with the higher-lying ^1P state, which is in accordance with above-discussed efficiency of the radiation trapping.

The present measurement of values for $(n_1L)_{\text{av}}$ and determination of number densities $(n_1)_{\text{av}}$ in the four lowest-lying helium excited states was performed applying the OES method, where the effect of simultaneous emission and absorption along the plasma column generated in a capillary DBD was utilized. Bearing in mind the pulsed working regime, the obtained number densities are related to time-averaged values during the 2 μs long discharge pulses with the frequency of 21.5 kHz, where the shape of voltage pulses was nearly sinusoidal.

The investigations of the He metastable density (n_m) in atmospheric He DBDs, performed previously by other authors,^{26–29} are related to the triplet $2s\ 2^3\text{S}_1$ state. Nersisyan et al.²⁶ and Tachibana et al.²⁷ performed the LAS measurements at 388²⁶ and 1083 nm²⁷ in planar atmospheric helium DBD, and found the densities $n_m < 2 \times 10^{10} \text{ cm}^{-3}$ and $n_m \sim 1 \times 10^{11} \text{ cm}^{-3}$, respectively.

The determination of n_m in a capillary atmospheric helium DBD was reported Urabe et al.^{28,29} The metastable density was measured by LAS at 1083 nm transition with capillaries of different inner diameter (1.25 to 4 mm), and metastable density in the DBD jet was determined to be $n_m \sim 1 \times 10^{11} \text{ cm}^{-3}$.

It is hard to make straightforward comparison of the results obtained with different DBDs because it is known that the properties of DBDs depend on many parameters, among

others, on size and geometry of the electrodes. However, our present results for the density of the He metastable $2s\ 2^3\text{S}_1$ state in the DBD capillary are consistent with those reported previously for the density in DBD jet.^{28,29} The He metastables He_m^* in the jet are subject to rapid destruction in collisions with nitrogen molecules in the air due to the Penning ionization process $\text{He}_m^* + \text{N}_2 \rightarrow \text{He} + \text{N}_2^+$, and it is plausible that their number density is significantly lower than in the capillary.

CONCLUSION

Optical emission spectroscopy was used to determine the populations of the lowest excited helium states $2s\ ^3\text{S}_1$, $2s\ ^1\text{S}$, $2p\ ^3\text{P}_J$ and $2p\ ^1\text{P}^0$ created in an atmospheric helium capillary DBD. The intensities of He lines emitted at 388, 501, 587, and 667 nm were measured side-on and end-on with respect to the discharge axis. The intensities observed end-on exhibited absorption in the line kernels due to simultaneous emission and absorption along the plasma column length L , while the side-on spectra were optically thin. This difference was utilized in the analysis of the experimental and theoretical line profiles. By fitting the measured profiles into the field of the profiles calculated for a series of n_1L values corresponding to the conditions in the experiment, the n_1L for the particular investigated state was determined. The emission profiles were measured as a function of the discharge voltage in the range covering homogeneous as well as filamentary DBD operation mode. Due to nonuniformity of the excited atom density distribution along the plasma, the average values of n_1 could be obtained only in the homogeneous operation mode where the nonuniformity was small. The following maximum values for the average populations along the plasma column in the capillary were determined: $n_1^{\text{av}}(2s\ ^3\text{S}_1) = (2.9 \pm 1.1) \times 10^{13} \text{ cm}^{-3}$, $n_1^{\text{av}}(2s\ ^1\text{S}) = (1.4 \pm 0.5) \times 10^{13} \text{ cm}^{-3}$, $n_1^{\text{av}}(2p\ ^3\text{P}_J) = (1.1 \pm 0.4) \times 10^{13} \text{ cm}^{-3}$, $n_1^{\text{av}}(2p\ ^1\text{P}^0) = (4.2 \pm 1.6) \times 10^{12} \text{ cm}^{-3}$.

To our knowledge, there are no results available in the literature on the determination of the populations created in the He $2s\ ^1\text{S}$ metastable, the $2p\ ^1\text{P}^0$ resonance, and the $2p\ ^3\text{P}_J$ states.

The method presented here for the determination of atom number densities by means of OES can be very useful in the situations when standard LAS measurements cannot be done, either due to lack of radiation sources for the excitation at a particular wavelength or when optical paths are too short to produce measurable absorption.

ASSOCIATED CONTENT

Supporting Information

Fine structures of multiplet 388 and 587 nm lines, corresponding spectroscopic parameters, and the data relevant for the fitting procedure. This material is available free of charge via the Internet at <http://pubs.acs.org>.

AUTHOR INFORMATION

Corresponding Author

*E-mail: franzke@isas.de.

Notes

The authors declare no competing financial interest.

ACKNOWLEDGMENTS

Financial support by the Ministerium für Innovation, Wissenschaft und Forschung des Landes Nordrhein-Westfalen, the Bundesministerium für Bildung und Forschung, the

Deutsche Forschungsgemeinschaft (project No. FR 1192/13-1) and the Ministry of Science, Education, and Sports of the Republic of Croatia (project No. 035-0352851-2853) is gratefully acknowledged.

■ REFERENCES

- (1) Na, N.; Zhao, M.; Zhang, S.; Yang, C.; Zhang, X. *J. Am. Soc. Mass Spectrom.* **2007**, *18*, 1859–1862.
- (2) Harper, J. D.; Charipar, N. A.; Mulligan, C. C.; Zhang, X.; Cooks, R. G.; Ouyang, Z. *Anal. Chem.* **2008**, *80*, 9097–9104.
- (3) Wiley, J. S.; Garcia-Reyes, J. F.; Harper, J. D.; Charipar, N. A.; Ouyang, Z.; Cooks, R. G. *Analyst* **2010**, *135*, 971–979.
- (4) Jackson, A. U.; Shum, T.; Sokol, E.; Dill, A.; Cooks, R. G. *Anal. Bioanal. Chem.* **2011**, *399*, 367–376.
- (5) Huang, M. Z.; Jhang, S. S.; Cheng, C. N.; Cheng, S. C.; Shiea, J. *Analyst* **2010**, *135*, 759–766.
- (6) Zhang, Y.; Ma, X. X.; Zhang, S. C.; Yang, C. D.; Ouyang, Z.; Zhang, X. R. *Analyst* **2009**, *134*, 176–181.
- (7) Liu, Y. Y.; Lin, Z. Q.; Zhang, S. C.; Yang, C. D.; Zhang, X. R. *Anal. Bioanal. Chem.* **2009**, *395*, 591–599.
- (8) Michels, A.; Tombrink, S.; Vautz, W.; Miclea, M.; Franzke, J. *Spectrochim. Acta, Part B* **2007**, *62*, 1208–1215.
- (9) Vautz, W.; Michels, A.; Franzke, J. *Anal. Bioanal. Chem.* **2008**, *391*, 2609–2615.
- (10) Olenici-Craciunescu, S. B.; Michels, A.; Meyer, C.; Heming, R.; Tombrink, S.; Vautz, W.; Franzke, J. *Spectrochim. Acta, Part B* **2009**, *64*, 1253–1258.
- (11) Hayen, H.; Michels, A.; Franzke, J. *Anal. Chem.* **2009**, *81*, 10239–10245.
- (12) Chan, G. C. Y.; Shelley, J. T.; Wiley, J. S.; Engelhard, C.; Jackson, A. U.; Cooks, R. G.; Hieftje, G. M. *Anal. Chem.* **2009**, *83*, 3675–3686.
- (13) Müller, S.; Krähling, T.; Veza, D.; Horvatic, V.; Vadla, C.; Franzke, J. *Spectrochim. Acta, Part B* **2013**, *85*, 104–111.
- (14) Kunze, K.; Miclea, M.; Musa, G.; Franzke, J.; Vadla, C.; Niemax, K. *Spectrochim. Acta, Part B* **2002**, *57*, 137–146.
- (15) Tachibana, K.; Kishimoto, Y.; Sakai, O. *J. Appl. Phys.* **2005**, *97*, 123301/1–123301/7.
- (16) Horvatic, V.; Müller, S.; Veza, D.; Vadla, C.; Franzke, J. *J. Anal. At. Spectrom.* **2014**, DOI: 10.1039/c3ja50343g.
- (17) Müller, S.; Krähling, T.; Veza, D.; Horvatic, V.; Vadla, C.; Franzke, J. *Spectrochim. Acta, Part B* **2013**, *85*, 104–111.
- (18) HemC, R.; Michels, A.; Olenici, S. B.; Tombrink, S.; Franzke, J. *Anal. Bioanal. Chem.* **2009**, *395*, 611–618.
- (19) Thorne, A.; Litzén, U.; Johanson, S. *Spectrophysics—Principles and Applications*; Springer-Verlag: Berlin–Heidelberg, Germany, 1999.
- (20) Wiese, W. L.; Smith, M. W.; Glennon, B. M. *Atomic Transition Probabilities*; National Standard Reference Data Series, U.S. Government Printing Office: Washington D. C., 1966; Vol. 1
- (21) Phelps, A. V. *Phys. Rev.* **1955**, *99*, 1307–1313.
- (22) Holstein, T. *Phys. Rev.* **1951**, *83*, 1159–1168.
- (23) Gallagher, A. In *Atomic, Molecular & Optical Physics Handbook*; Drake, G.W.F., Ed.; AIP Press: Woodbury, NY, 1966; pp 220–232.
- (24) Möllisch, A. F.; Oehry, B. P. *Radiation Trapping in Atomic Vapours*; Clarendon Press: Oxford, U.K., 1998.
- (25) Vadla, C.; Horvatic, V.; Niemax, K. *Spectrochimica Acta, Part B* **2003**, *58*, 1235–1277.
- (26) Nersisyan, G.; Morrow, T.; Graham, W. G. *Appl. Phys. Lett.* **2004**, *85*, 1487–1489.
- (27) Tachibana, K.; Kishimoto, Y.; Sakai, O. *J. Appl. Phys.* **2005**, *97*, 123301/1–123301/7.
- (28) Urabe, K.; Morita, T.; Tachibana, K.; Ganguly, B. N. *J. Phys. D: Appl. Phys.* **2010**, *43*, 095201/1–095201/13.
- (29) Urabe, K.; Motomura, H.; Sakai, O.; Tachibana, K. *J. Phys. D: Appl. Phys.* **2011**, *44*, 042001/1–042001/5.